Quasi-static indentation response of pedestrian bridge multicellular pultruded GFRP deck panels

L.S. Sutherland, M.F. Sá, J.R. Correia, C. Guedes Soares, A. Gomes, N. Silvestre

Abstract

This paper presents an experimental study of the *quasi*-static indentation behaviour of a pultruded glass fibre reinforced polymer (GFRP) multicellular deck panel used in footbridges. To simulate the applied loads to be experienced by such a deck during its service life, various sets of specimens extracted from the panel cross-section were perforated statically across its top flange thickness using different indenters. Load-displacement responses, failure modes and absorbed energies were analysed concerning the influence of the following parameters: (i) specimen geometry (single laminated flange, 1-cell and 3-cells); (ii) indenter type (size – 6/10 mm and shape – hemispherical/flat), and (iii) damage protection (surface coating and filling of the section cavities with polyurethane foam). The results obtained show that simpler specimen geometries are able to predict the quasi-static indentation behaviour of the bridge deck in particular cases and for specific measured responses; nonetheless, they are not able to simulate the effects of damage protections. The application of a surface coating proved to be the only successful protection method in delaying the first significant damage, giving higher absorbed energy levels. However, regarding the onset of perforation, both protection strategies considered did not provide any appreciable improvement. The results obtained also show that penetration failure modes due to “standard” high-heel loads are not likely to occur on the bridge deck even if its surface is not protected. Nevertheless, in this case, both initial damage and perforation may be easily inflicted by heavier pedestrians walking or running upon “stiletto-type” high-heels.

Keywords

Multicellular footbridge deck, pultruded GFRP laminate, Mechanical static testing, Static indentation

1. Introduction

Fibre reinforced polymer (FRP) materials are being increasingly used in civil engineering applications owing to their numerous advantages over traditional materials, such as reinforced concrete and steel, namely their high specific strength and stiffness, lightness, ease of erection, improved durability and low maintenance [1]. Among the different types of FRP materials commercially available, pultruded glass fibre reinforced polymer (GFRP) components are particularly well suited for bridge structures [2], where they are generally used in the following formats: (i) GFRP bars for concrete reinforcement [3]; (ii) GFRP profiles for bridge girders [4]; and (iii) GFRP panels for bridge decks [5]. GFRP panels are used for the decks of both pedestrian and vehicular bridges, for both new constructions and rehabilitation of existing structures. In general these panels are of a multicellular pultruded cross-section, interconnected using adhesive bonding and/or mechanical interlocking [6]. A recent example of this type of construction is the 13.6 m span S. Mateus Footbridge in

Viseu, Portugal (see Fig. 1) [1]. The 75 mm thick GFRP deck panels of this bridge, representative of most multicellular decks used in footbridges, are the subject of this paper.

Fig. 1. S. Mateus GFRP-steel hybrid footbridge, Viseu, Portugal [1].

Important design constraints for GFRP bridge decks include deflections (both initial and due to creep) stemming from the low stiffness and viscoelasticity of the pultruded material [1–3], and the dynamic response to vibrations due to passing pedestrians and/or vehicles due to the low density and reduced damping [7]. The relatively thin cross-sectional cell walls of the multicellular pultruded panels generally used in this type of application (<5 mm thick in this case), together with the very thin coating/finishing layers applied, mean that susceptibility to local *out-of-plane* indentation and/or impact loads is an important additional concern. Typical examples of high local concentrated loads include those due to high heels, umbrella ferrules, acts of vandalism, tool drops during installation, or even floating debris during extreme flooding. These concerns are compounded by the fact that FRP materials are known to be susceptible to this type of loading and that the fibre architecture of pultruded sections includes a high proportion of unidirectional reinforcement in the pultruded/longitudinal direction, which is known to be especially susceptible to this kind of damage (Abrate [8]). Similar concerns exist with the application of FRP multicellular panels for road bridges when subjected to the effects of concentrated tyre load [9,10].

One of the first studies on the static indentation behaviour of GFRP pultruded members was presented by Found et al. [11]. The authors tested three different glass-polyester laminates (thicknesses of 4.75 mm and 6.35 mm) obtained from flat sheets or webs of I-section profiles (fibre volume fraction approximately 35%). The authors tried to correlate the damage in the lower surface of the specimens (in terms of cracking) with the permanent indentation of the contact surface. They concluded that the damage caused by static indentation was more severe than that due to impact, suggesting that the type of loading governs the development of the damage and that the damage is not just dependent on the force.

Tabiei et al. [12] studied the impact behaviours of GFRP pultruded box (50.8 × 50.8 × 3.18 mm, single cell) beams made of either polyester or vinylester with a fibre volume content of approximately 30%. The authors conducted both static tests and impact

tests at different velocities in order to determine the loading rate sensitivity of the beams. The ultimate load measured in the static tests was comparable to that obtained from the impact tests, where it was found to decrease with the impact velocity. Specimens made of vinylester resin presented better performance for all impact velocities and were also those in which the ultimate load was less sensitive to the impact velocity.

Tabiei et al. [13] pursued the previous study in a set of GFRP beams – single and multi-cell tubes (open and closed cross-sections, minimum thickness of 3 mm) – forming pultruded 'building blocks', for use as roadside safety barriers. Both *quasi*-static and impact tests were conducted in order to optimize the impact performance of a full-scale prototype guardrail, defined in terms of maximum strength and energy absorption. Closed cross-sections presented better performance than open ones, namely higher maximum loads and less brittle failures. Moreover, the failure mechanism of beam barriers with more internal webs and individual cells was more favourable, with higher load capacity for longer durations. Such better performance should be attributed to the internal redundancy of those cross-sections.

Furthermore, it is important to note that the consideration of the effects of highly concentrated local loading is not considered by the relevant construction standards and design codes. The most highly 'concentrated' loads considered are those acting over a relatively large area; for example, according to Eurocode 0 [14], a load of 10 kN applied over a deck surface of 0.10 m^2 should be considered in the design of pedestrian bridges. Since the response and the damage incurred due to an impact 'event' will depend on the specific characteristics of the event considered, it is imperative to choose a specific 'event' that will give a typical severe case for simulation in the laboratory environment so that test results are relevant to 'real life'. In this case, a suitable 'worst case' event is that of a pedestrian in high-heeled shoes. The next step in assessing the effects of impact is to ensure that experimental conditions correspond to those in operation in a given type of application. Various technical guidelines [15,16] and previous studies [17–19] addressing human comfort to footbridge vibrations provide relevant information about local loads induced by pedestrians. Fig. 2 illustrates the dependence of a 'load dynamic factor' (peak force/static weight) and contact time as a function of the pacing frequency (step/s) for slow walking to running [20].

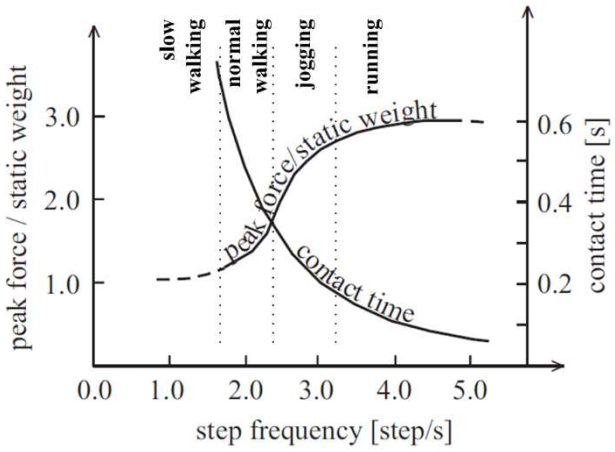

Fig. 2. Load dynamic factor and contact time as a function of step frequency. Adapted [20].

Fig. 2 shows that at a normal walking frequency of around 2 steps/s, dynamic effects lead to an exerted load of approximately 1.5 times the static weight of the pedestrian, and that whilst running (4 steps/s), the dynamic force can be over 3 times the static body weight. For a pedestrian of 75 kg walking on a typical high-heel of cross-sectional area of 1 cm^2 this would lead to contact pressures of over 10 MPa and 20 MPa for walking and running respectively. For a 75 kg person running in a "stiletto" style high-heel (≈0.4 cm^2), this corresponds to a pressure of nearly 56 MPa. The next step is to ensure that the rates of force application are relevant to real life. Winter [21] states that for natural cadence (*i.e.*, steps/min) '*at HC [Heel Contact] both vertical and horizontal velocity are near zero*' and in fact goes onto say that, '*to refer to this event as heel strike is quite erroneous*'. This suggests that, although perhaps counterintuitive, a *quasi*-static response would be most relevant to the problem of "high-heel impacts".

Hence, the overall aim of this study is to investigate the behaviour and failure of pultruded GFRP panels used in pedestrian bridge decks subjected to *quasi*-statically applied concentrated loads, which should simulate those to be experienced during the daily use of the bridge by pedestrians.

2. Experimental programme

2.1. Materials

The materials used in the experimental programme were: (i) the GFRP pultruded material used to construct the actual bridge; (ii) rigid polyurethane lightweight foam, and (iii) a two-layer polymeric floor coating (non-slip), for the latter two materials see Section 2.4. The GFRP material used in the experimental programme is a pultruded multicellular deck panel manufactured by *Kookmin Composite Infrastructure Inc.*, South Korea. The deck panels with a length of 2.5 m (in the pultrusion direction) have a cross-section comprised of two panel faces (upper and lower flanges) joined by vertical laminate walls (webs) [1]. Conceived as successive 'I-beams', the cross-section hence contains seven tubular cavities with the following nominal dimensions: height of 75 mm, width of 90 mm, and wall thickness of 4 mm (see Fig. 3). At the web-flange junctions the flange thickness is slightly higher at around 5 mm. Along the panel edges there are two vertical asymmetric snap-fit interlocks allowing for the successive assembly of adjacent parallel deck panels.

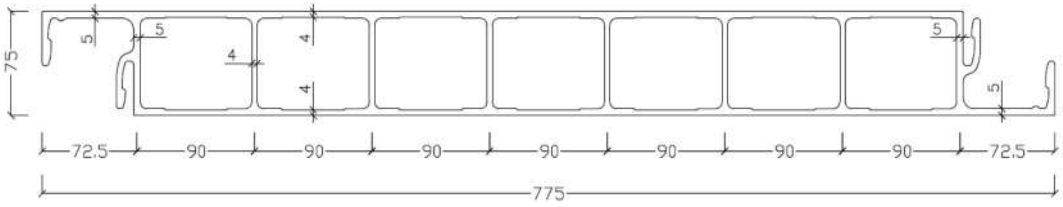

Fig. 3. Cross-section geometry of the multicellular GFRP deck panel (dimensions in *mm*).

The pultruded material is made of an isophthalic polyester matrix reinforced with layers of E-glass rovings and multi-axial stitched fabrics in the bulk of the laminates. Chopped strand mats (450 g/m^2) are also used at the outermost layers of the deck (to improve waterproofing) and at the snap-fit edges (to provide local strengthening) [1]. The inorganic content of the GFRP material is 67% (by weight), a value obtained through burn-off tests [22] performed on small-scale coupons cut from both the webs and flanges of the deck

panel sections. The material density is 18.6 kN/m^3 corresponding to a deck weight per unit area of 26 kgf/m^2.

2.2. 'Base-line' test setup

To achieve the two main overall aims of this part of the study, an *Instron* 1343 universal test machine was used to apply a concentrated load laterally to the centre of the pultruded GFRP members, as shown in Fig. 4a. The specimens were simply supported on a very stiff solid 20 mm thick steel base. A 3-cell configuration of length 200 mm in the pultrusion direction (Fig. 4b.1) was considered here as a reasonable "base-line" representation of the actual cross-section of the seven cells of a whole panel (see Fig. 3).

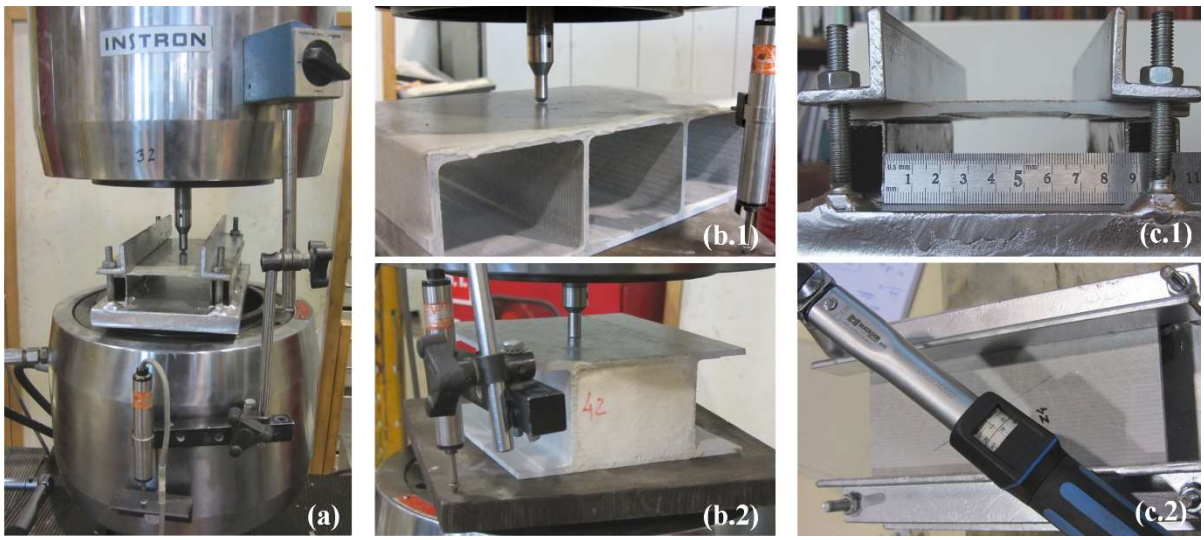

Fig. 4. Test setups: (a) *Instron* universal test machine, (b.1-2) load application on cellular specimens and (c.1-2) supporting and clamping system for the laminated plate specimens.

The concentrated load was applied via a stainless steel 'indenter'. As a reasonable simulation of a severe in-use event (*e.g.*, high-heel) a 10 mm diameter hemispherical indenter was used (Fig. 5a). A load application rate of 0.1 mm/s was used since it gave an extremely low strain rate as compared to typical impact tests, whilst giving a practical test time. Load and displacement (from the point of first contact with the specimen) of the indenter were measured and recorded. All tests were conducted until the total perforation of the specimen.

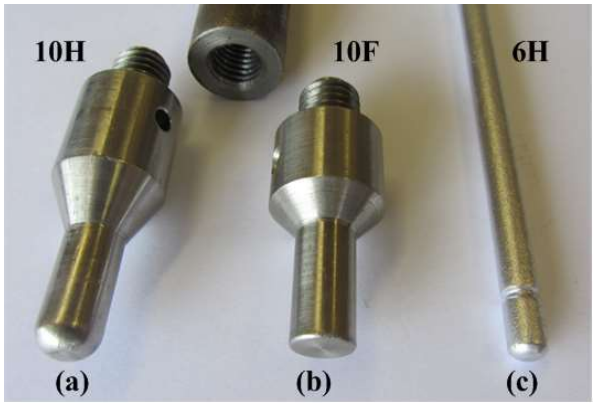

Fig. 5. Indenters: (a) 10 mm hemispheric, (b) 10 mm flat and (c) 6 mm hemispheric.

2.3. Specimen geometry screening

Because the number of deck panels available for this experimental study was limited, various test specimen geometries were considered in order to try to economise on the amount of material required. However, it was imperative that the geometry considered simulated in a sufficiently accurate manner the behaviour of the actual footbridge deck cross-section, since previous investigation has shown that the behaviour may well be highly dependent upon the test set-up [23]. All specimens were produced with the same length dimension of 200 mm in the pultrusion/longitudinal direction. The specimen geometries considered were:

(i) One cell width denominated by '1C' in Fig. 6a, and shown under test conditions in Fig. 4b.2 (NB: in this figure the specific specimen shown is foam filled as described in Section 2.4);

(ii) Three cell widths, the 'base-line' specimen (Section 2.2) denominated by '3C' in Fig. 6b, and shown under test conditions in Fig. 4b.1;

(iii) A fully clamped section of the cell flange (upper) laminate, denominated by 'LA' in Fig. 6c, and shown under test conditions in Fig. 4a (often referred to as a *shear punch test*). The detail of the clamping arrangement, illustrated in Fig. 4c, included securing bolts tightened to 15 N m as measured using a torque wrench to ensure a consistently well-clamped specimen in each case.

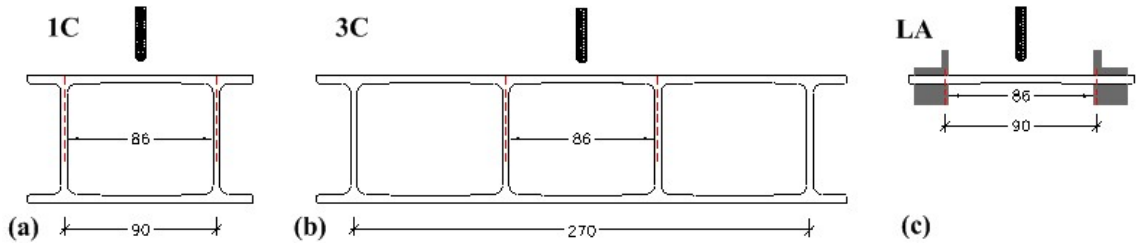

Fig. 6. Specimen geometries: (a) 1-cell, (b) 3-cell and (c) clamped laminate (dimensions in *mm*).

2.4. Damage protection

Additionally, the possibility of enhancement of the resistance to damage due to concentrated loads was considered via two methods of protection:

(i) Polyurethane foam filling of the GFRP section cells (foam, 'PU');
(ii) Application of a protective layer to the specimen upper surface (coating, 'CO').

A rigid polyurethane foam was used to fill the cavities of selected '1C' and '3C' specimens (clearly this was not possible for the 'LA' specimens). Isocyanate and polyol fluid components in a 1:1 ratio were injected into the cells, combining to give foam which expanded to fill the cells. The foam data sheet [24] states a density of 45 kg/m^3 and a compressive strength of 200 kPa; the compressive Young's modulus was measured as 5.6 MPa.

A non-slip resin coating with 1.5–2.0 mm of thickness was applied to the upper face of selected specimens, see Fig. 7. This consisted of an initial coat of 'Sikafloor 156' epoxy resin [25] followed by inorganic silica sand (of size range 0.1–0.3 mm) and a surface coat of

'Sikafloor 400 N elastic' polyurethane resin paint [26]. The former resin is a bi-component chemical hardener with density of 1.1 kg/l and compressive strength of 60 MPa, whilst the latter is a one-component chemical liquid with 1.6 kg/l of density (both curing at 23 °C and 50% HR).

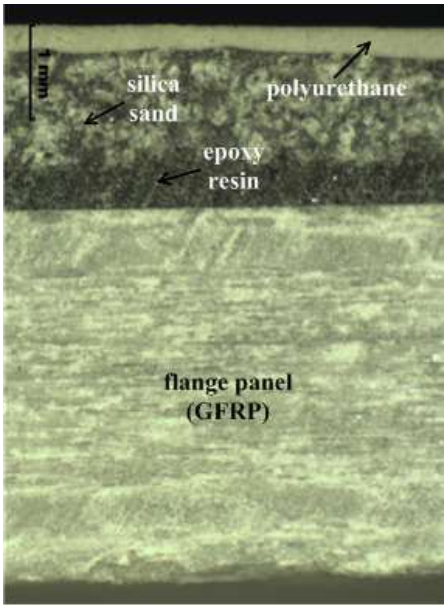

Fig. 7. Non-slip resin coating surface (zoom detail).

2.5. Sensitivity to indenter type (size & form)

Previous experience has shown that the size and shape of the indenter can significantly influence the behaviour seen [27]. Also, the concentrated load events likely to be suffered by the bridge are varied, especially in the size and shape of the object (*e.g.*, high-heel, umbrella ferule, dropped objects). Although it is not feasible to study all possibilities in the current study, an initial investigation into this effect was made by also considering two additional indenters, giving:

(i) The 'base-line' 10 mm diameter hemispherical indenter (Fig. 6a);
(ii) The 10 mm diameter flat indenter (Fig. 6b);
(iii) The 6 mm diameter hemispherical indenter (Fig. 6c).

2.6. Experimental design

Hence, we now have an experimental study involving three parameters or 'factors', each of which can take one of three values or 'levels', as shown in Table 1. Since the effects of the various parameters for such a loading have been shown to be highly dependent on the values taken by the other parameters (*i.e.*, there are significant 'interaction effects'), it would have been desirable to carry out tests at every combination of each of the values of each of the parameters. However, this would have led to a test programme involving 27 permutations. Also, the testing of composite materials usually leads to a high degree of statistical scatter, which requires replications of each factor-level combination, or experimental 'run', to be made. Hence, due to the restricted amount of test material available only a carefully designed subset of the full factor-level combinations was considered.

Factor	Levels & Denominations		
Specimen geometry	'3C' (3-cell)	'1C' (1-cell)	'LA' (laminate)
Damage protection	'NP' (no protection)	'PU' (foam)	'CO' (coating)
Indenter type	'10H' (10 mm hemispheric)	'10F' (10 mm flat)	'6H' (6 mm hemispheric)

Table 1. Experimental parameters ('factors'), and values assigned ('levels') with their denominations.

Firstly, the combination of clamped laminate with PU foam is not physically possible. Secondly, the combination of one cell width with coating ('1C-CO') was not considered since the one cell (unprotected) configuration was found to give an invalid failure mode, as described in Section 3.2. Thirdly, the effect of indenter size and form was only investigated at one value of each of the three parameters, namely 1-cell with foam ('1C-PU'), 3-cell with no foam or no coating protection ('3C-NP'), and clamped laminate with no foam or coating protection ('LA-NP'). This gave a total of 13 test setups, as shown in Table 2. Three replicate tests were carried out for each setup, giving a full experimental programme of 39 tests.

		Specimen geometry		
		1C (1-cell)	**3C** (3-cell)	**LA** (laminate)
Damage protection	**NP** (no protection)			
	PU (foam)	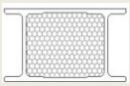	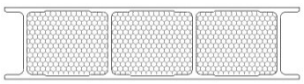	–
	CO (coating)	–		

NOTE: shaded configurations tested with indenters '10H', '10F' & '6H', other configurations tested with indenter '10H' only.

Table 2. Test matrix: specimen geometry *vs*. damage protection (*Inc.* indenter type).

3. Results

3.1. Load-displacement behaviour

The load-displacement (test machine cross-head displacement) behaviours seen all showed a common progression as illustrated in Fig. 8. The individual behaviours of each specimen are then given in Figs. 9 and 10 for the 10 mm hemispherical indenter and for the 6 mm hemispherical and 10 mm flat indenters, respectively. There is no plot for the unprotected single cell tests since (as discussed in Section 3.2) this specimen geometry resulted in an invalid failure mode.

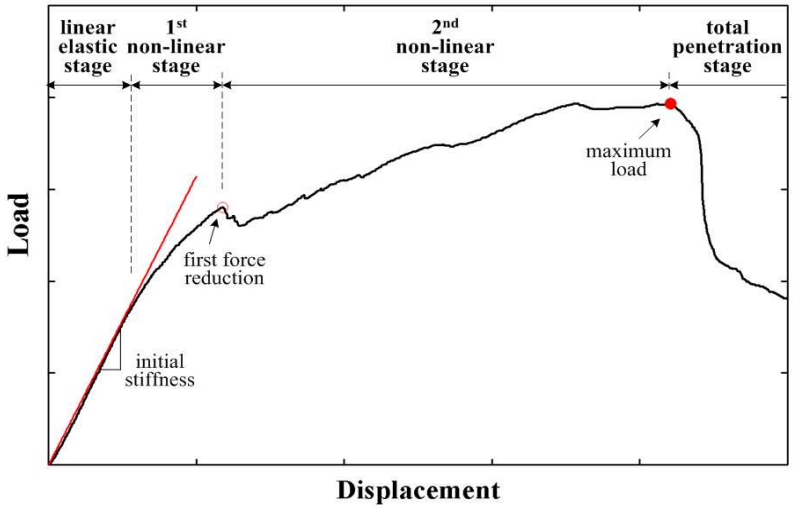

Fig. 8. Typical *load-displacement* behaviour curve with notable stages assigned.

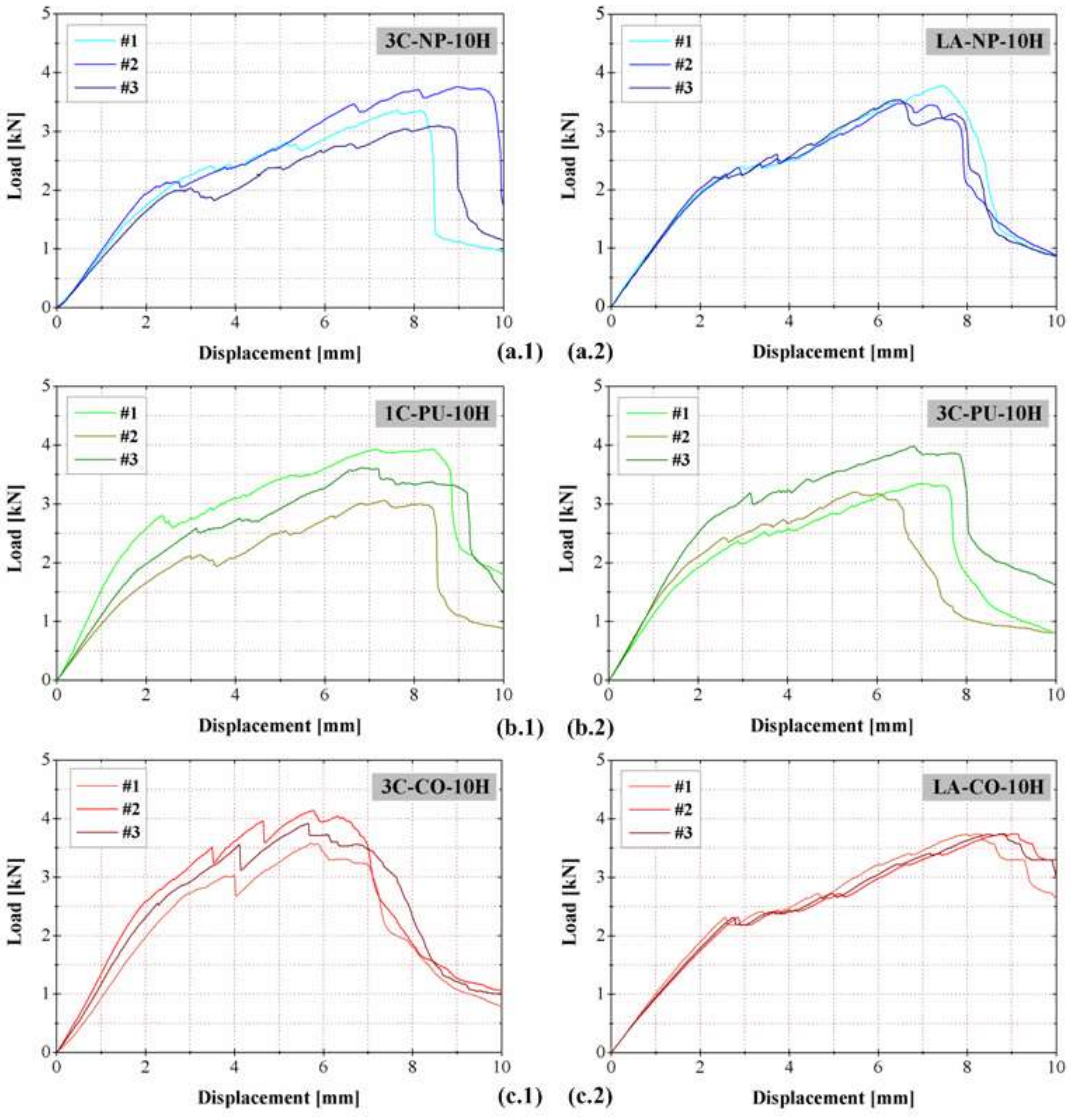

Fig. 9. *Load-displacement* curves of specimens with (a-c) 10 mm hemispherical indenter: (a) 3C and LA unprotected specimens, (b) 1C and 3C foam specimens and (c) 3C and LA coated specimens.

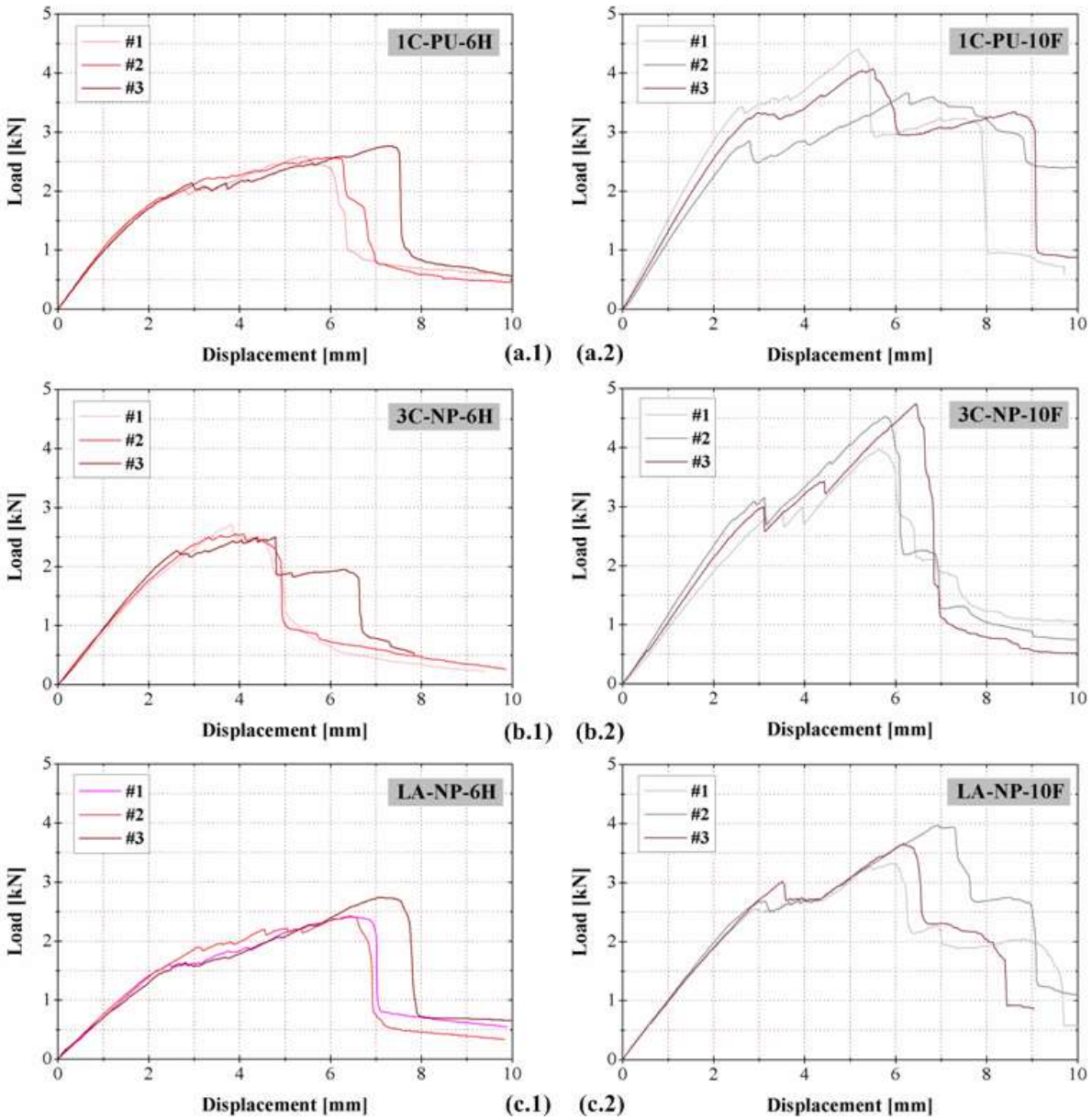

Fig. 10. *Load-displacement* curves of specimens with (a.1–c.1) 6 mm hemispherical and (a.2–c.2) 10 mm flat indenters: (a) 1C foam specimens, (b) 3C unprotected specimens and (c) LA unprotected specimens.

The initial '*linear elastic*', constant stiffness stage ended with a progressive reduction in stiffness – the '*1st non-linear stage*', which was very short for the LA specimens and longer for the 1C and 3C specimens. Then a slight but marked reduction in force occurred at the '*load at first force reduction*'. This event corresponded to the first visible damage suffered by the specimens due to (audible) cracking and delamination of the upper surface – '*damage initiation*'.

The load then increased again during a '*2nd non-linear stage*' where further small load reductions occurred as the laminate was progressively penetrated until a '*maximum load*', corresponding to the *perforation* of the specimen (*total penetration*), was reached. Subsequently the load continuously decreased as the indenter emerged from the other side of the laminate during the '*total penetration stage*'. Table 3 summarizes the average values

of initial elastic stiffness, load at first force reduction, maximum load and the corresponding displacement, and the total energies (*i.e.*, both elastically and irreversibly due to damage) absorbed by the specimens up to the load at first force reduction and up to the maximum load. Absorbed energy values were obtained via integration of the force-displacement data.

Specimen [factor]			Initial elastic stiffness	Load at 1st force reduction	Maximum load	Displacement at maximum load	Absorbed energy to 1st force reduction	Absorbed energy to maximum load
Geometry	**Protection**	**Indenter**	[kN/mm]	[kN]	[J]	[mm]	[J]	[J]
1C (1-cell)	**NP** (no protection)	**10H**	(0.73 ± 33%)	(1.96 ± 16%)	(2.41 ± 15%)	(7.83 ± 09%)	(3.78 ± 49%)	(14.02 ± 04%)
	PU (foam)	**10H**	1.20 ± 28%	2.49 ± 15%	3.54 ± 13%	7.07 ± 03%	4.06 ± 14%	16.98 ± 12%
		6H	1.00 ± 03%	2.02 ± 06%	2.64 ± 04%	6.19 ± 15%	3.56 ± 18%	12.19 ± 22%
		10F	1.32 ± 12%	3.20 ± 10%	4.04 ± 09%	5.62 ± 10%	5.20 ± 09%	15.42 ± 05%
3C (3-cell)	**NP** (no protection)	**10H**	0.95 ± 10%	2.17 ± 10%	3.40 ± 10%	8.36 ± 08%	3.60 ± 38%	19.83 ± 11%
		6H	0.91 ± 05%	2.29 ± 05%	2.59 ± 04%	4.17 ± 13%	4.01 ± 09%	8.08 ± 31%
		10F	1.08 ± 10%	2.97 ± 04%	4.41 ± 09%	5.96 ± 07%	5.01 ± 02%	14.87 ± 16%
	PU (foam)	**10H**	1.26 ± 09%	2.56 ± 13%	3.51 ± 12%	6.41 ± 13%	4.21 ± 07%	16.07 ± 18%
	CO (coating)	**10H**	1.22 ± 15%	3.37 ± 09%	3.88 ± 07%	5.69 ± 08%	8.02 ± 07%	14.87 ± 12%
LA (laminate)	**NP** (no protection)	**10H**	1.02 ± 03%	2.34 ± 03%	3.60 ± 04%	6.83 ± 08%	4.18 ± 08%	17.12 ± 12%
		6H	0.69 ± 06%	1.70 ± 10%	2.53 ± 07%	6.64 ± 05%	2.67 ± 21%	11.69 ± 05%
		10F	0.96 ± 02%	2.73 ± 10%	3.65 ± 09%	6.29 ± 09%	4.81 ± 20%	15.02 ± 10%
	CO (coating)	**10H**	1.05 ± 09%	2.45 ± 06%	3.81 ± 04%	7.80 ± 06%	3.73 ± 05%	19.67 ± 12%

NOTE: values for 1-cell unprotected specimens (1C-NP-10H, in parentheses) not considered as valid results due to failure mode (see Section **Error! Reference source not found.**).

Table 3. Experimental elastic stiffness, load, displacement and absorbed energy at 1st force reduction and at maximum load (*average* ± *cv.*).

3.2. Failure modes

The failure modes observed are now described in correspondence with the *load–displacement* behaviours of the previous section; firstly, the sequence of events observed in the tests of the 'base-line' specimens (3C-NP-10H) is described in detail, and then differences in the failure modes caused by specimen geometry, protection and indenter changes are briefly discussed.

Even during the initial '*linear elastic stage*' of the 'base-line' specimens, before any significant damage was seen, some audible cracking was often heard right from the earliest stages of the test. This was largely attributed to the localized compression of the top flange due to the initial contact of the indenter head. Then, coincident with the '*1st non-linear*

stage' with increasing load the audible cracks became louder and were seen to be due to the superficial cracking of the top face (Fig. 11i). Such cracking was almost parallel to the pultrusion direction, due to damage at the matrix-reinforcement interface following the high proportion of unidirectional reinforcement in this direction. At the '*1st force reduction*', although not visible, it is very probable that this sudden force reduction and the associated stiffness reduction was due to sudden internal delamination as repeatedly observed for the corresponding stiffness reductions seen in previous work on marine laminates [23,27,28]. With the progress of indentation, the internal rovings of the laminate suffered increasing fibre breakage. This progressive damage (Fig. 11ii), which is well reflected in the '*2nd non-linear stage*' of the specimens' response, continued until perforation of the specimen by the indenter – the '*total penetration stage*' (Fig. 11iii). This last stage was defined here as starting at the maximum load, and is accompanied by a continued reduction in force as the indenter progressively passed through the laminate.

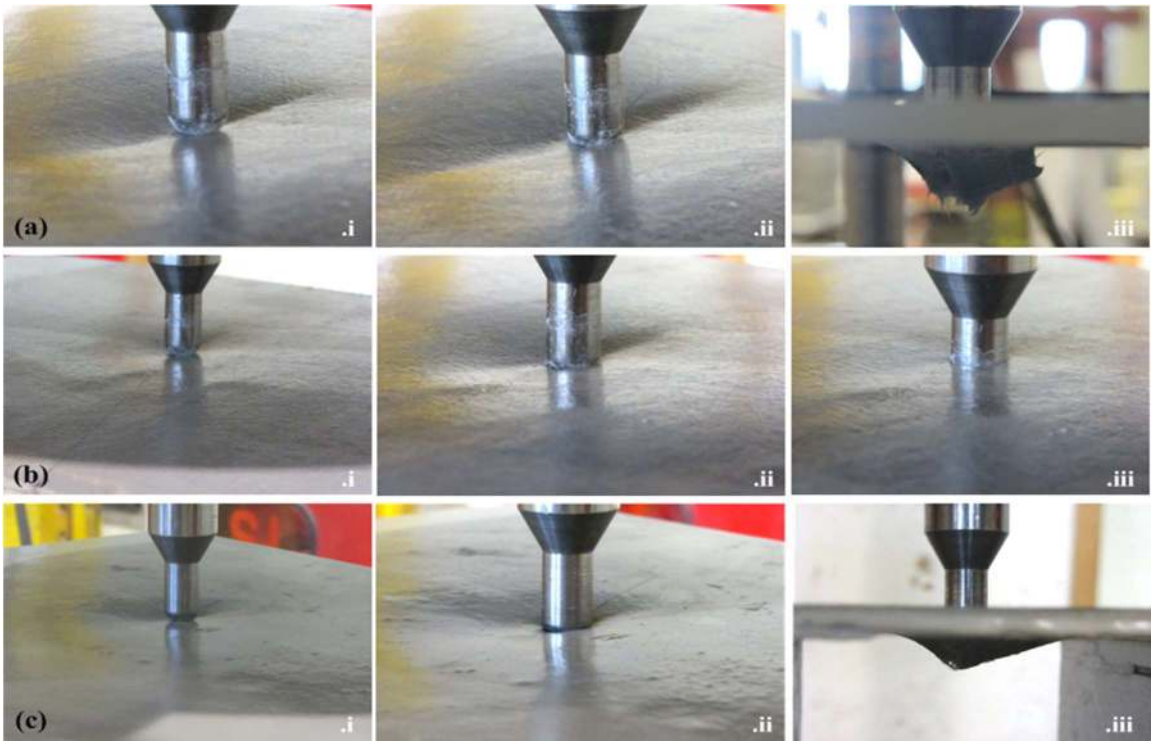

Fig. 11. *Quasi-static* indentation frame sequence of the 'base-line' (a) unprotected, (b) foam and (c) coated specimens: (i) pre 1st nonlinear regime, (ii) penetration initiation and (iii) progression of penetration.

Concerning the influence of specimen geometry, the overall failure mode of the laminated specimens was similar to that of the 'base-line' 3-cell configuration (see Fig. 12). Conversely, the 1C specimens suffered a very different failure mode, failing at the web-top/flange junctions due to excessive rotation of the loaded laminate, with an associated folding failure along the centre of the laminate before perforation could occur (see Fig. 13). However, the supporting action of the foam in the 1C foam protected geometry avoided this unwanted failure mode (see Fig. 14).

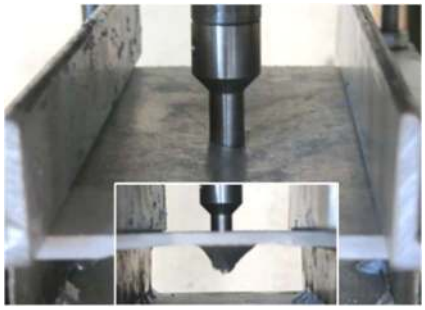

Fig. 12. Perforation failure mode of a laminated uncoated specimen.

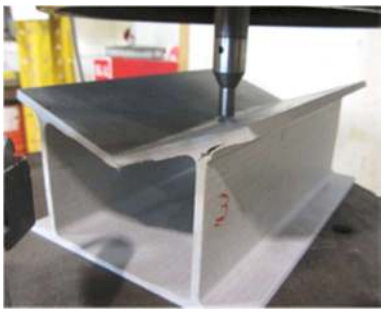

Fig. 13. Flexural failure of a 1-cell unprotected specimen.

Fig. 14. Perforation failure mode of a 1-cell foam protected specimen.

Considering the effect of the damage protection, the main differences in failure modes were both twofold and similar for both protections tested (PU foam and non-slip coating): (i) the audible cracks at the first stage of the test were less intense; and (ii) the cracks observed at the top face were fewer and less aligned with the pultrusion direction. These effects of damage protection were relatively consistent for each of the different specimen geometries. Finally, despite the differences in local contact stress distributions, the changes introduced in the indenter geometry did not cause significant differences in the sequence of the different stages described above for the 'base-line' specimens. However, locally the extent of the damaged zone did vary, decreasing with the diameter reduction of the hemispherical indenter from 10 to 6 mm, as expected, although the failure modes were equivalent (see Fig. 15a and b). Using a flat indenter gave a 'punched disk' failure and a more elongated 'splitting' type failure on the front and back faces, respectively (Fig. 15c).

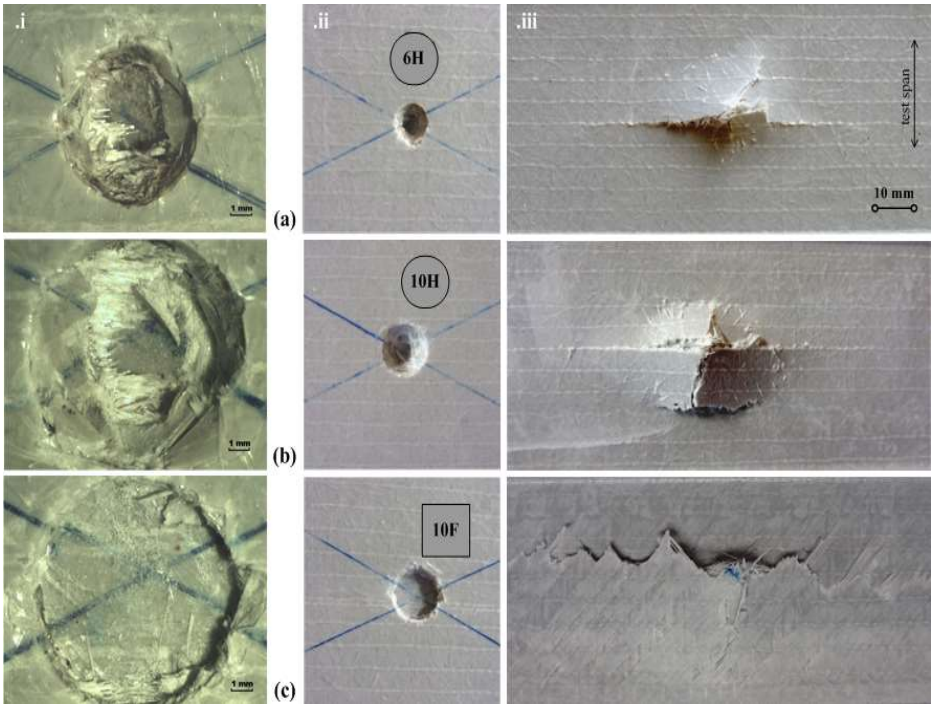

Fig. 15. Local failure zones of the 3-cells unprotected specimens for indenters (a) 6H, (b) 10H and (c) 10F: (i) zoomed view of front face by binocular loupe, and normal views of (ii) *front face* and (iii) *back face*.

4. Discussion

The audible cracks and decreasing stiffness of the 1st non-linear stage indicate that some minor internal damage occurs before damage or perforation becomes visible at the surface, and this is thought to be due to matrix cracking. As encountered in previous work [23,27,28] the first load drop is almost certainly correlated with the onset of the first significant damage; in this case the indenter was seen to progressively penetrate the surface during the markedly less stiff 2nd non-linear stage, and the previous work indicates that internal (and hence hidden) delamination could also well be at least partially responsible for this stiffness reduction. However, although further work would be required to identify exactly which damage mode or modes has or have occurred here, whichever the damage modes this is most definitely the first significant damage in terms of degradation of structural performance.

Table 3, together with Figs. 9 and 10 show that the results obtained were consistent, particularly for the clamped plate geometry which exhibited very low variability; most likely due to the simpler geometry and well defined boundary conditions. The one exception to this is the results for the 1-cell specimens which gave a higher degree of scatter due to the invalid failure modes suffered. Overall, values pertaining to perforation were generally more variable than those of the linear elastic and 1st and 2nd non-linear stages.

For a multi-parameter problem study such as this the effects on a measured ‘response’ of one parameter may well not be equal at each of the values of the other parameters. In the terminology of experimental design, this is termed ‘interaction’ between two parameters. A very concise and clear method of presenting such complex behaviours is through ‘interaction plots’ (see [29] for an introduction to these concepts) which is used below to

identify and describe the effects of and interactions between the parameters considered here for the various responses measured.

4.1. Effects of specimen geometry and damage protection

The three plots of Fig. 16 show the effect of the various protections on the initial stiffness, load at 1st load reduction and maximum load for each of the specimen geometries considered tested with indenter 10H.

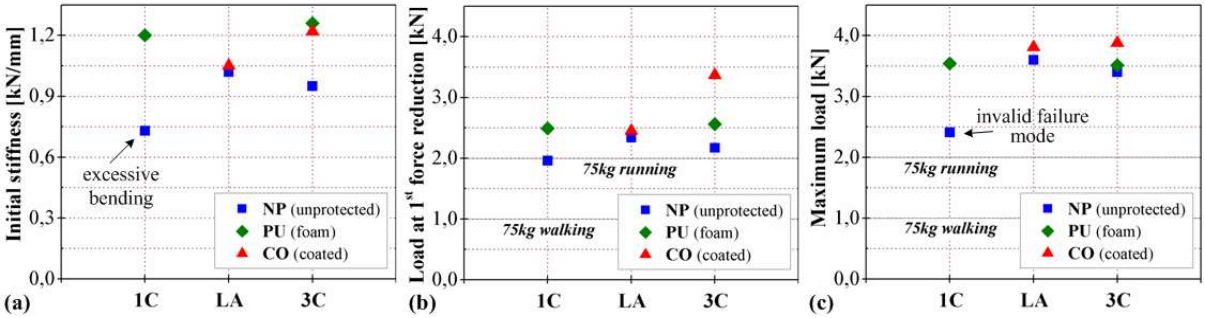

Fig. 16. Geometry-protection interactions (indenter 10H): (a) initial stiffness, (b) load at 1st force reduction and (c) maximum load.

Fig. 16a and c show that the initial stiffness and maximum load of the unprotected 1C specimens was markedly less than for the other two specimen geometries. This corresponds with the observation of the invalid failure mode due to excessive bending of the flange described in Section 3.2. This further confirms that this specimen geometry should not be used to predict the behaviour of the bridge pultrusions themselves. However, Fig. 16b shows that the load corresponding to the onset of the first significant damage to the 1C unprotected specimens is not so greatly reduced compared to that of the other geometries, doubtless because this damage occurs before the invalid failure seen at higher loads.

Conversely, the three plots of Fig. 16 show that for a foam-filled section the 1C configuration gives very good estimates of the 3C behaviour for initial stiffness, load at 1st load reduction and maximum load. This was due to the support to the upper flange offered by the foam thus preventing the invalid failure mode observed in the unprotected 1C specimens. The same figures also show that, for unprotected specimens, the clamped laminate configuration gives slightly higher values for the same three responses than measured for the ‘base-line’ 3C geometry.

The effect of the application of a protective coating to the clamped laminated plates did not significantly change any of the responses plotted in Fig. 16, whereas both coating and foam filling the 3C specimens generally increased these responses although each response was affected in a different way. For these last specimens, Fig. 16a shows that the surface coating and foam-filling both increased the initial stiffness by a significant margin and by a very similar amount (a relative increase of about 30%). Fig. 16b shows that the load to first significant damage was greatly increased (1.6 times) by the application of a coating, but that foam filling the section was not quite so successful in delaying this initial failure (1.2 times increase). Note that for the ‘base-line’ configuration, the average stiffness during the non-linear stage (*cf*. Fig. 9, reflecting both global and local indentation deformations) increased for both types of protection. Fig. 16c shows that foam filling did not significantly increase the maximum load corresponding to perforation (3% relative difference) and that applying a

surface protection led only to a small increase (about 14%) in this response. These observations correspond to the expectations that both protections could potentially increase resistance to initial damage, but that their influence on full penetration, *i.e.* perforation, would not be significant.

The load required to initiate different types of damage can easily be related to the load expected from a given individual walking on the bridge deck, but the energy absorbed up to the initiation of damage is also another useful criterion of the resistance to damage. Hence, similar interaction plots for the absorbed energy responses are shown in Fig. 17, also for the 10H indenter. Since these figures are obtained through integration of the force-deflection plots, the energy absorbed is dependent not only on the loads reached, but also on the form of these force-deflection plots.

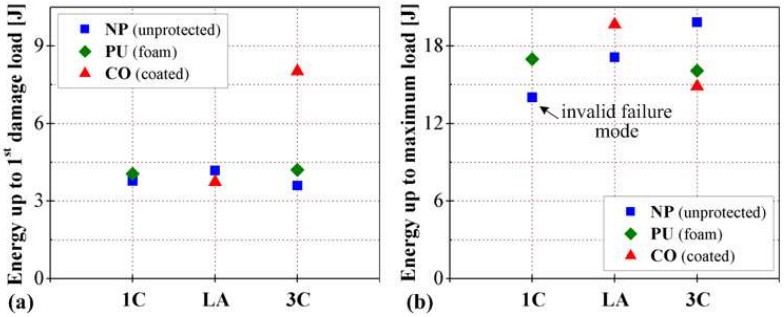

Fig. 17. Geometry-protection interactions for the absorbed energy up to: (a) 1st force reduction and (b) maximum load.

Fig. 17a shows that the application of a surface coating to the 3C specimens significantly increased the energy absorbed up to the first significant damage, indicating that this was a particularly successful protection strategy. In all other cases this energy was seen to be independent of both the different specimen geometries and protection. However, in Fig. 17b the energy absorbed up to the maximum load, corresponding to the perforation, of the 3C specimens was decreased both by the application of a coating and by filling them with foam; indicating that these protection strategies actually reduced the resistance to *perforation*. Conversely, in Fig. 17b a surface coating increased the energy absorbed up to perforation for the clamped laminate. However, since Fig. 17a and b show that the only case where the energy absorbed by the 3C specimens was correctly predicted by the laminated plate geometry was that up to initial damage for the unprotected case, this latter effect is not of practical interest.

4.2. Effects of indenter size and geometry

The plots of Figs. 18 and 19 show the effect of changing the indenter geometry or diameter on the initial stiffness, load at 1st load reduction, maximum load, energy absorbed up to 1st load reduction and energy absorbed up to maximum load for the unprotected clamped plate and 3C specimen geometries. Since the failure mode of the 1-cell unprotected geometry was found to be invalid for the 10 mm diameter hemispherical indenter, these points are not included in these figures and the effect of changing the indenter for this specimen geometry was not investigated.

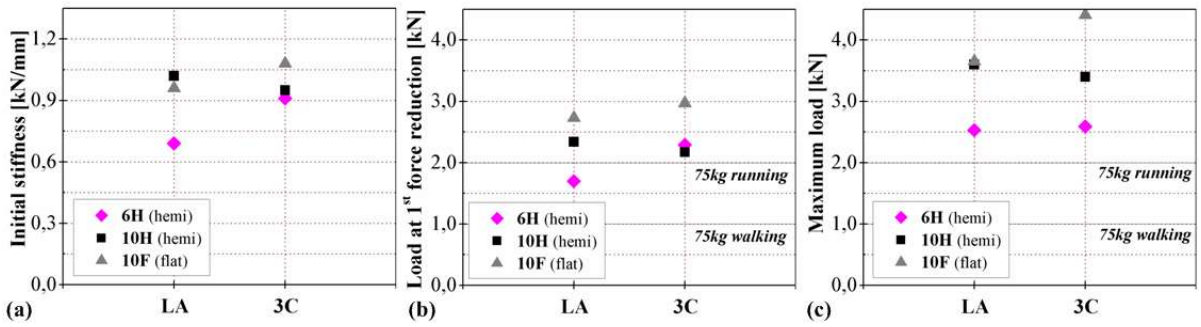

Fig. 18. Geometry-indenter interactions: (a) initial stiffness, (b) load at 1st force reduction and (c) maximum load.

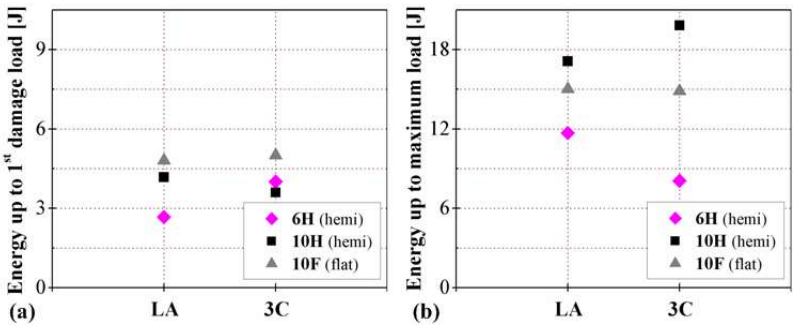

Fig. 19. Geometry-indenter interactions for the absorbed energy up to: (a) 1st force reduction and (b) maximum load.

For the 3C specimens the initial stiffness and the load and absorbed energy up to the first damage are unaffected by a decrease in the diameter of a hemispherical indenter from 10 mm to 6 mm, indicating that initial failure is unaffected by this magnitude of diameter reduction. However, the same decrease in indenter diameter results in a significant decrease in the maximum load reached and a very large decrease in the amount of energy absorbed up to this load, indicating that perforation is very much influenced by this magnitude of diameter reduction.

The use of a 10 mm indenter with a flat instead of hemispherical end results in higher values of all responses except for absorbed energy up to maximum load which shows a significant reduction. This indicates that the resistance to initial damage due to a flat indenter is higher than that due to a hemispherical one, but that penetration starts earlier with a flat indenter.

The capability of the clamped plate geometry to correctly predict the various responses of the ‘base-line’ 3-cell geometry for each indenter is given in Table 4, which shows that the use of a clamped plate is only advisable for a small number of response-indenter combinations.

Response / Indenter	6 mm Hemi	10 mm Hemi	10 mm Flat
Initial elastic stiffness (kN/mm)	-24%	7%	-11%
Load at 1st force reduction (kN)	-26%	8%	-8%
Energy to 1st force reduction (J)	-33%	16%	-4%
Maximum load (kN)	-2%	6%	-17%
Energy to maximum load (J)	45%	-14%	1%

Table 4. Geometry-indenter interactions: % error from clamped plate to 3-cell geometry test results.

4.3. Practical interpretations

From the ratios of dynamic to static reaction forces given in the introduction (see Fig. 2), a pedestrian of 75 kg walking at a normal frequency of around 2 steps/s would exert a force of approximately 1 kN, and of over 2 kN whilst running at 4 steps/s (as indicated by the horizontal dotted lines in Figs. 16 and 18). For the following discussion only the base-line 3-cell geometry is considered as the best approximation to the bridge pultrusions themselves.

Fig. 16c shows that even for somebody running the penetration loads for a 10 mm hemispherical-ended indenter are not reached by a safe margin (relative and absolute differences of 70% and 1.4 kN respectively, for a 75 kg pedestrian). Although the base of a high-heel is not hemispherical, this severe case geometry is thought to be suitably indicative of that of a flat-based high-heel contacting, as is perhaps normal, at an angle without the associated rotation moments which would cause inaccuracies in the measurements or even damage to the test machine. However, Fig. 16b shows that an unprotected pultrusion would be very susceptible to initial damage by the same running pedestrian, and that although a coating would safely shield the surface, filling the sections with PU foam would not be significantly successful.

A flat indenter, corresponding more to a high-heel placed exactly upright (perhaps unlikely in normal walking) reduces the danger of both initial and perforation damage as seen in Fig. 18b and c. Conversely, a reduction in the diameter of the high-heel to ‘stiletto-type’ dimensions would result in a great danger of not only of initial damage but also of perforation of the deck laminate by a running pedestrian if the surface was not protected.

Although the discussions above that a smaller and more concentrated loading indenter increases the likelihood of damage is perhaps intuitive, they do show that in this specific ‘in service’ application under every-day loadings these types of damage are very possible, and also that appropriate surface protection could be used to mitigate these dangers. Further, if a heavier pedestrian or increased loadings from events such as stumbling are encountered, the equivalent horizontal dotted lines in Figs. 16 and 18 will be at higher loads and hence damage may also be quite conceivably suffered even when walking.

It is well worth noting that although the initial damage sites are likely to be small, they are also likely to be; (i) difficult to detect (initial damage) or conversely unsightly (perforation), (ii) very numerous and hence with a cumulative degradative effect, and (iii) likely nucleates

for delamination extension due to repeated cyclic global loadings, which may ultimately affect the overall integrity of the bridge itself.

5. Conclusions

A large number of quasi-static indentation tests on the pultruded GFRP multicellular sections of an in-service pedestrian bridge have been completed. The effects of specimen geometry and indenter diameter and form were investigated systematically. Load on and deflection of the indenter were measured, and then integrated to give the energy absorbed by the specimens. An initial 'linearly elastic stage' gave way to a '1st non-linear' stage as stiffness progressively reduced, which itself finished with a distinct '1st force reduction' associated with the onset of initial damage. As damage increased a '2nd non-linear stage' progressed until a maximum load was reached as perforation (full penetration) of the laminate occurred.

Although the base of a high-heel is not hemispherical, this severe case geometry is thought to be suitably indicative of that of a flat-based high-heel contacting at an angle. Further work exploring the effect of using indenters of different geometries and of materials used to fabricate high heels would be beneficial. Material saving specimen geometries may be used to predict the behaviour of the bridge deck pultrusions in specific cases for specific measured responses, but they will not predict well trends in terms of the effects of protection methods. The 1-cell geometry should not be considered due to non-valid deformations and final failure mode.

The application of a surface coating to the 3-cell specimens had a significant effect on the energy absorbed up to the first significant damage, indicating that this would be a successful protection strategy in delaying initial damage. As expected, neither of the protection strategies considered appreciably increased resistance to perforation.

A decrease in the diameter from 10 mm to 6 mm of the hemispherical indenter used did not affect the onset of initial failure, but perforation was initiated earlier with the smaller diameter. The resistance to initial damage due to a flat indenter is higher than that due to a hemispherical one, but conversely, resistance to perforation is lower with a flat indenter.

Although for somebody running in a 'standard' high-heel the loads produced would not cause penetration, an unprotected pultrusion would be very susceptible to initial damage. A coating would safely shield the surface, but filling the sections with PU foam would not be significantly successful. A running pedestrian wearing 'stiletto-type' high-heels could easily inflict both initial damage and perforation if the surface was not protected. Walking heavier pedestrians or events such as stumbling may also easily damage the unprotected GFRP deck.

Finally, it is worth noting that other typical concentrated load events (*e.g.*, umbrella ferrules, dropped objects) could also be a cause for concern and would be considered as 'low-velocity' impact events where '*the contact duration is long enough for the entire structure to respond to the impact*' [30]. Hence further work investigating the impact response of the same pultrusions is also to be published in the future. The results from the current paper are of great use in estimating the incident impact energies required up to damage and perforation of the specimens under dynamic impact tests; previous experience [27] has

shown that *quasi*-static results can be used to give conservative estimates of these impact energies.

Acknowledgements

The authors would like to thank CERIS-ICIST and FCT for funding this investigation. The second author also gratefully acknowledges the financial support provided by FCT, through the doctoral scholarship n° SFRH/BD/42798/2007. This work was also supported by FCT, through IDMEC, under LAETA, project UID/EMS/50022/2013.

References

[1] Sá MF (2015); "Analysis of pultruded GFRP multicellular decks panels – application to pedestrian bridges". *PhD Thesis in Civil Engineering*. IST, University of Lisbon [*in Portuguese*].

[2] Keller T (2003); "Use of fibre reinforced polymers in bridge construction". *In Structural Engineering Documents*, 7, IABSE, Zurich.

[3] Bank LC (2006); "Composites for Construction: Structural Design with FRP Materials". *John Wiley & Sons*, Hoboken, New Jersey.

[4] Gonilha JA, Correia JR, Branco FA (2014); "Structural behaviour of a GFRP-concrete hybrid footbridge prototype: Experimental tests and numerical and analytical simulations". *Engineering Structures*, 60: 11–22.

[5] Knippers J, Pelke E; Gabler M; Berger D (2010); "Bridges with Glass Fibre–Reinforced Polymer Decks: The Road Bridge in Friedberg, Germany". *Structural Engineering International*, 20(4): 400–404.

[6] Lee SW, Hong KJ, Park S (2010); "Current and Future Applications of Glass-Fibre-Reinforced Polymer Decks in Korea". *Structural Engineering International*, 20(4):405–408.

[7] Bai Y, Keller T (2008); "Modal parameter identification for a GFRP pedestrian bridge". *Composites Structures*, 82(1): 90–100.

[8] Abrate S (1998); "Impact on Composite Structures". *Cambridge University Press*, Cambridge UK.

[9] Majumadar PK, Lesko JJ, Cousins TE, Liu Z (2009); "Conformable tire patch loading for FRP composite bridge deck". *Journal of Composites for Construction*, 13(6):575–581.

[10] Sebastian WM, Webster T, Kennedy C, Ross J (2013); "Profiled metal plate – Cork mat loading systems on cellular FRP bridge decks to reproduce tyre-to-deck contact pressure distributions". *Construction and Building Materials*, 49: 1064-1082.

[11] Found MS, Holden GJ, Swamy RN (1997); "Static indentation and impact behaviour of GRP pultruded sections". *Composite Structures*, 39(3-4): 223–228.

[12] Tabei A, Svansod A, Hargravec M (1996); "Impact behaviour of pultruded composite box beams". *Composite Structures*, 36: 155–160.

[13] Tabei A, Svansod A, Hargravec M, Bank L (1998); "Impact performance of pultruded beams for highway safety applications". *Composite Structures*, 42: 231–237.

[14] CEN EN 1990-A2 (2005); "Eurocode 0: Basis of structural design – Annex A2: Applications for bridges" (Normative). *Comité Européen de Normalisation* (CEN), Brussels.

[15] SÉTRA – Service d'Études Techniques des Routes et Autoroutes (2006); "Footbridges – Assessment of vibrational behaviour of footbridges under pedestrian loading". *Technical guide*.

[16] SYNPEX – European Project (2007); "Advanced load models for synchronous pedestrian excitation and optimised design guidelines for steel footbridges". Project RFS-CR 03019, Final Report, *Research Fund for Coal and Steel* (RFCS).

[17] Bachmann H, Amman W (1987); "Vibrations in structures induced by man and machines". In *Structural Engineering Documents*, 3, IABSE, Zurich.

[18] Bachmann H (1992); "Case studies of structures with man-induced vibrations". *Journal of Structural Engineering*, 118(3): 631–647.

[19] Nimmen KV, Lombaert G, Roeck G, Broeck PV (2014); "Vibration serviceability of footbridges: Evaluation of the current codes of practice". *Engineering Structures*, 59: 448–461.

[20] Zivanovic S, Pavic A, Reynolds P (2005); "Vibration serviceability of footbridges under human induced excitation: A literature review". *Journal of Sound and Vibration*, 279(1-2): 1–74.

[21] Winter DA (2005); "Biomechanics and Motor Control of Human Movement". *John Wiley & Sons*, 3rd Ed. Hoboken, New Jersey.

[22] ISO 1172 (1996); "Textile-glass-reinforced plastics – Prepregs, moulding compounds and laminates – Determination of the textile-glass and mineral filler content: Calcination methods". *International Organization for Standardization* (ISO), Genève.

[23] Sutherland LS, Guedes Soares C (2003); "The effects of test parameters on the impact response of glass reinforced plastic using an experimental design approach". *Composites Science and Technology*, 63:1–18.

[24] Synthesia Española – Ficha de produto (2007); "Sistema de colada 481-N y 481L-N".

[25] SIKA Portugal, SA – Ficha de produto (2008); "Sikafloor® 156". Nº ID: 8.32, nº 8.

[26] SIKA Portugal, SA – Ficha de produto (2007); "Sikafloor® 400 N Elastic". Nº ID: 8.02, nº 6.

[27] Sutherland LS, Guedes Soares C (2012); "The use of quasi-static testing to obtain the low-velocity impact damage resistance of marine GRP laminates". *Composites Part B: Engineering*, 43(3): 1459–1467.

[28] Sutherland LS, Guedes Soares C (2006); "Impact behaviour of typical marine composite laminates". *Composites Part B: Engineering*, 37(2–3):89–100.

[29] Sutherland LS, Shenoi RA, Lewis SM (1998); "Size and scale effects in composites: II unidirectional laminates". *Composites Science and Technology*, 59:221–233.

[30] Richardson MOW, Wisheart MJ (1996); "Review of low velocity impact properties of composite materials". *Composites Part A*, 27(12): 1123–1131.